Soft Matter

Cite this: *Soft Matter*, 2012, **8**, 7243

www.rsc.org/softmatter

PAPER

Stalk-free membrane fusion of cationic lipids *via* an interdigitated phase

Georg Pabst,*[a] Caroline Lonez,[b] Michel Vandenbranden,[b] Jacques Jestin,[c] Aurel Radulescu,[d] Jean-Marie Ruysschaert[b] and Thomas Gutberlet[e]

Received 22nd March 2012, Accepted 24th April 2012
DOI: 10.1039/c2sm25665g

We have studied the membrane structure of a cationic lipid (*N*-*t*-butyl-*N*′-tetradecyl-3-tetradecylaminopropionamidine, termed diC14-amidine) using X-ray and neutron small-angle scattering as well as dilatometry and ultrasound velocimetry. At high temperatures we found an anomalously thin lamellar fluid phase, which transforms into a loosely packed interdigitated phase below the chain melting transition. Our finding can be understood based on the specific structure of the lipid backbone, which forms a long spacer between the alkyl chains. The loose lipid packing in the gel phase leads to a significant exposure of the hydrophobic lipid core to the aqueous phase. This reduces energy penalties from the removal of water molecules during fusion and explains the untypically increased fusion properties of amidine in the gel phase. Moreover, this fusion in the gel interdigitated state apparently does not require the formation of stalk intermediate structures.

Introduction

Cationic lipids form various aggregate structures when complexed with DNA, due to an intricate interplay of electrostatic interactions,[1–6] and are useful agents for DNA transfection.[7–11] Structural properties of these complexes examined by using small-angle X-ray scattering (SAXS) measurements revealed a lamellar or hexagonal phase organization.[2,5] *N*-*t*-Butyl-*N*′-tetradecyl-3-tetradecylamino-propionamidine (termed diC14-amidine or Vectamidine) (Fig. 1A)[12] is a cationic lipid that transfects DNA and mRNA into mammalian cells with high efficiency[12–15] and stimulates immune responses.[15–18] Moreover, as compared to most cationic lipids, diC14-amidine does not require a helper lipid to form efficient lipoplexes, which was explained by the preferred cone-like molecular shape of the lipid and the related propensity for negative curvature.[19]

DNA/diC14-amidine lipoplexes were studied previously by various biophysical techniques,[20–24] revealing that the structures of the complexes are mainly governed by electrostatic interactions, similar to observations in other lipoplexes.[1,2,4–6] In particular, X-ray scattering studies showed that diC14-amidine lipoplexes form a bilayer structure with sandwiched DNA strands in the fluid phase.[22] In the absence of DNA, diC14-amidine was found to exhibit a main phase transition at 21 °C,[25] which is close to that of dimyristoyl phosphatidylcholine (DMPC) (Fig. 1B).[26] However, the transition width is much broader and hence less cooperative as compared to the zwitterionic lipid. Spin-label electron resonance spectroscopy experiments further revealed the influence of pH on the melting transition,[27] which is due to the titratable amine and amidine groups leading to two distinct pK_a values.[20]

Interest in the physicochemical properties of diC14-amidine has been spurred most recently by an about fivefold increased fusion capability in the gel phase transition, in contrast to the temperature-dependence of other fusogenic lipids.[25] Moreover, based on a comparison of the spectroscopic properties of diC14-amidine with those of the chain analogue DMPC (Fig. 1B), the same study suggested the formation of an interdigitated gel phase.[25] The correlation to the jump of fusogenic properties of diC14-amidine at the main phase transition suggests a tight link between the two observations. However, lipid mediated membrane fusion is

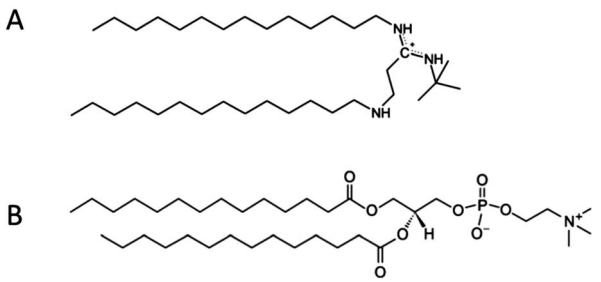

Fig. 1 Molecular structures of diC14-amidine at pH = 7 (A) and dimyristoyl phosphatidylcholine (DMPC) (B).

[a]*Institute of Biophysics and Nanosystems Research, Austrian Academy of Sciences, Schmiedlstr. 6, 8042 Graz, Austria. E-mail: georg.pabst@oeaw.ac.at; Fax: +43 316 4120 390; Tel: +43 316 4120 342*
[b]*Laboratory for Structure and Function of Biological Membranes, Centre for Structural Biology and Bioinformatics, Faculté des Sciences, Université Libre de Bruxelles, CP 206/2, Campus Plaine, Blvd. du Triomphe, 1050 Brussels, Belgium*
[c]*Laboratoire Léon Brillouin, CEA/CNRS, C.E.A Saclay, 91191 Gif-sur-Yvette Cedex, France*
[d]*Forschungszentrum Jülich GmbH, Jülich Centre for Neutron Science, Lichtenbergstr. 1, 85747 Garching, Germany*
[e]*Helmholtz-Zentrum Berlin GmbH, Hahn-Meitner-Platz 1, 14109 Berlin, Germany*

typically considered to take place *via* the formation of stalk intermediate structures, where two leaflets of two opposing lipid bilayers are merged *via* point-like defects.[28–30] Such a mechanism is not conceivable in chain interdigitated membranes, where the two bilayer leaflets are merged. Henceforth, detailed knowledge of the involved structural parameters is indispensable to delineate the underlying physical mechanisms of membrane fusion from an interdigitated phase. For this purpose, we have combined X-ray and neutron scattering as well as dilatometry and ultrasound velocimetry. We found a loosely packed interdigitated phase $L_{\beta I}$ below the chain melting transition and an anomalously thin L_{α} phase above, which can be explained by the chemical structure of the lipid backbone. Our results suggest a fusion mechanism based on lipid dissolution from the interdigitated membranes without the formation of stalk intermediates.

Materials and methods

Sample preparation

DiC14-amidine was synthesized as described previously.[12] To form liposomes, diC14-amidine was dissolved in chloroform, dried under a nitrogen stream, and left overnight under vacuum to remove all traces of solvent. Liposomes were then formed at 56 °C by addition of pre-heated buffer (10 mM Hepes, pH 7.3) to the pre-heated lipid film. After 10 min incubation, liposomes were vortex mixed for 1 min. Prior to each experiment, the liposomal suspension was heated at 56 °C for 10–15 min. Osmotically stressed samples were prepared by first centrifuging the hydrated liposomal dispersions (6000 rpm, 8 min) and then replacing the supernatant with a concentrated solution of polyethylene glycol (PEG, M_W = 8000). PEG was purchased from Sigma-Aldrich (St. Louis, MO). The final applied osmotic pressure was 8 atm.

For neutron scattering experiments, the dried diC14-amidine lipid film was dissolved in Hepes buffer prepared in D_2O (concentration: 5 mg ml^{-1}), otherwise following the same protocol detailed above.

Dilatometry and ultrasound velocimetry

The molecular volume of amidine and the propagation of ultrasound were determined using the DSA 5000 density and sound analyzer (Anton Paar, Graz, Austria). The instrument measures the density ρ of a solution *via* the vibrating tube principle, from which the partial specific molecular volume is obtained using[31]

$$\varphi_V = 1/\rho_0[1 - (\rho - \rho_0)/c], \quad (1)$$

with ρ_0 being the density of the reference solution (buffer) and c the lipid concentration (3 mg ml^{-1}). The molecular volume is then simply given by[32]

$$V = M_W\varphi_V/N_A, \quad (2)$$

where the molecular weight of diC14-amidine M_W = 535.9 and N_A is Avogadro's constant.

The DSA 5000 simultaneously measures the ultrasound velocity from which one derives the sound velocity number[32] using

$$[u] = (u - u_0)/(u_0c), \quad (3)$$

where u is the sound velocity of the sample and u_0 that of the reference solution. Further, one can define a volume expansion coefficient

$$\alpha = \Delta V/(V\Delta T) \quad (4)$$

as a measure for the thermal expansion. No fixed heating rate can be programmed with the DSA 5000. However from the speed of processing the temperature steps ΔT = 0.5 °C, we calculate an average scan rate of 0.07 °C min^{-1}.

Small and wide-angle X-ray scattering (SWAXS)

SWAXS experiments were performed using a compact Kratky camera (System 3, Hecus X-ray Systems, Graz, Austria) mounted on a sealed-tube generator (GE-Seifert, Ahrensburg, Germany). The generator was operated at 2 kW and CuK_{α} radiation (λ = 1.542 Å) was selected using a Ni-filter in combination with a pulse-height discriminator.

For measurements, samples were transferred into 1 mm thin-walled quartz capillaries and kept in good thermal contact with a Peltier unit during the experiments. The samples were exposed to an X-ray beam of size 0.5 mm × 3.5 mm ($V \times H$) for 3600 s and equilibrated for 600 s at each temperature. SWAXS patterns were recorded with two linear, one dimensional, position sensitive detectors (PSD 50, Hecus X-ray Systems, Graz, Austria) and calibrated using silver stearate and *para*-bromobenzoic acid.

From the WAXS peak observed below the melting transition we derived the lateral area per hydrocarbon chain from[33]

$$A_C = 8\pi^2/\left(\sqrt{3}q_{11}^2\right), \quad (5)$$

where q_{11} is the peak position of the orthorhombically packed chains.

Small-angle neutron scattering (SANS)

SANS experiments were performed using the KWS-2 high intensity/wide-q small angle neutron diffractometer of the Jülich Centre for Neutron Science (JCNS) at the research reactor FRM II (Garching, Germany) and at the PAXE SANS beamline at the Orphée reactor, Laboratoire Léon Brillouin CEA/CNRS (Gif-sur-Yvette Cedex, France).

Two separate detection/neutron wavelength configurations were used at both beamlines. The high q-range was measured at a sample/detector distance SD = 2 m, wavelength λ = 4.5 Å ($\Delta\lambda/\lambda$ = 20%) at KWS-2 and at SD = 1.5 m, λ = 6 Å ($\Delta\lambda/\lambda$ = 10%) at PAXE. The intermediate and low q ranges were measured at SD = 8 m at KWS-2 and 5.4 m at PAXE (same wavelengths as for high q). Data were collected with a 2-D detector system of 60 × 60 cm^2 based on a modified Anger technology with ^{6}Li glass as scintillator at KWS-2 and a BF_3 2-D neutron detector 64 × 64 cm^2 at PAXE.

At both beamlines samples were contained in 1 mm thick standard Hellma quartz cuvettes. Temperature control was provided by a circulating water bath. The 2-D raw data were corrected for the scattering from the empty cell, the solvent, and the electronic and background noise. The isotropic 2-D data

were integrated azimuthally to obtain the scattered intensity profile $I(q)$.

The reduced SANS data were modelled by

$$I(q) \propto F|(q)^2|/q^2, \quad (6)$$

where q is the scattering vector and the form factor was defined as

$$F(q) = d_{HC}\sin(qd_{HC}/2)/(qd_{HC}/2) \quad (7)$$

assuming a scattering length density of amidine in the form of a single step function, *i.e.* high density for buffer and headgroup and low density for the hydrocarbon regime in accordance with the contrast in D_2O. Then the parameter d_{HC} represents the thickness of the hydrocarbon membrane core.

Calculation of structural parameters

Following earlier work from Nagle and co-workers[34] we first determined the hydrocarbon volume per lipid in the gel phase

$$V_C^{gel} = 2A_C d_{HC}, \quad (8)$$

from which one simply gets the headgroup volume using the dilatometry data

$$V_H = V - V_C^{gel}. \quad (9)$$

Eqn (8) is valid only for interdigitated phases. For non interdigitated phases

$$V_C^{gel} = A_C d_{HC}. \quad (10)$$

This also serves as an independent check for the presence of an interdigitated phase, because application of eqn (10) produces negative V_H values if the chains interdigitate. It is reasonable to assume that the headgroup volume of amidine will not change upon the melting transition, as has been applied previously for phospholipids.[34–36] Thus, the fluid hydrocarbon volume is simply $V_C^{fluid} = V - V_H$, from which we then arrive at the lateral area per lipid in the fluid phase

$$A = 2V_C^{fluid}/d_{HC}. \quad (11)$$

Results

The molecular volume of diC14-amidine and its acoustic properties were measured as a function of temperature simultaneously. Experiments were repeated to ensure reproducibility. Fig. 2 shows the results for the partial specific volume, the sound velocity number as well as the volume expansion coefficient. All data exhibit significant changes at 21.6 °C, which corresponds to the melting transition of diC14-amidine and in good agreement with previous calorimetric data.[21]

The partial specific volume shows the typical step-like increase with $\varphi_V = 1.002$ mg ml^{-1} at 15 °C and $\varphi_V = 1.009$ mg ml^{-1} at 30 °C. These values can be compared to dilatometric data reported for phosphatidylcholines.[31,34] Interestingly, the values are more similar to those of dipalmitoyl phosphatidylcholine, $\varphi_V = 1.011$ mg ml^{-1} (50 °C), with 16 hydrocarbons per chain, than to its chain analogue dimyristoyl phosphatidylcholine

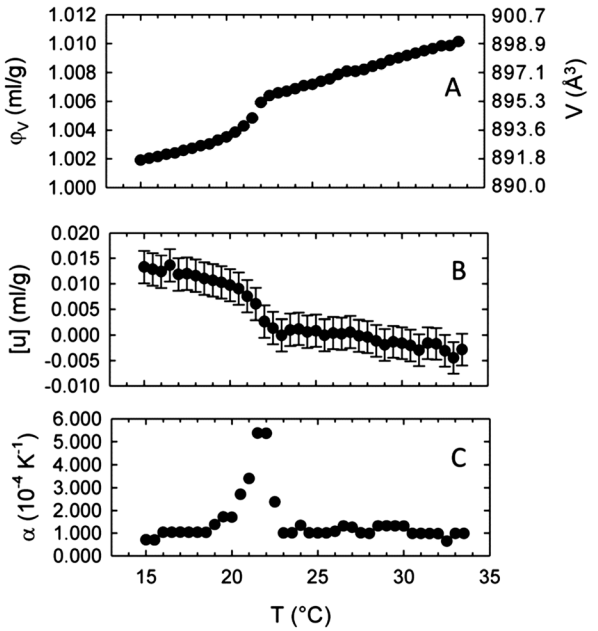

Fig. 2 Dilatometric and acoustic data of diC14-amidine as a function of temperature. Panel (A) shows the partial specific volume and also gives the corresponding molecular volume changes. Panel (B) gives the sound velocity number and panel (C) the volume expansion coefficient.

(DMPC), $\varphi_V = 0.977$ mg ml^{-1} (30 °C).[34] Due to the smaller molecular weight of diC14-amidine as compared to DMPC ($M_W = 677.9$) the molecular volumes are, however, smaller ($V^{DMPC} = 1100$ Å^3 (ref. 34), $V^{amidine} = 898$ Å^3 at $T = 30$ °C). This indicates a looser molecular packing of diC14-amidine as compared to that of phosphatidylcholines. We further note a small relative increase in lipid volume across the phase transition of ~0.3%. The typical relative increase in phospholipid volume across the main phase transition is 4%.[31,34]

The sound velocity number showed a typical dip at the transition point (Fig. 2B),[37] suggesting a drop of the bending rigidity at the transition point.[38] Compared to data available for DMPC,[37] $[u]$-values are ~10 times smaller. This indicates that diC14-amidine is significantly softer than DMPC.

The volume expansion coefficient of diC14-amidine exhibited a maximum at the main transition, from which we determined the transition temperature $T_m = 21.6$ °C, which agrees well with previous data.[25] The transition half width determined from the peak, $\Delta T_{1/2} = 1.2$ °C, is about 10 times broader than that of phosphatidylcholines.[39] Thus, the cooperative unit of diC14-amidine is small, in agreement with previously reported calorimetry data.[21,25] Hence, the dilatometric and acoustic data on diC14-amidine show that this lipid packs more loosely than other lipids and therefore forms a softer membrane.

To elucidate the structural basis for this behaviour, we performed SWAXS experiments. Because diC14-amidine has little electron contrast (three N per headgroup, Fig. 1), fully hydrated diC14-amidine liposomes exhibit only background scattering.[22] To circumvent this problem, we applied osmotic pressures of ~8 atm using PEG in order to transform the unilamellar diC14-amidine vesicles into a multilamellar arrangement. Fig. 3 gives an overview of the X-ray patterns in the small- and wide-angle

regime as a function of temperature. The SAXS regime exhibited a sharp peak with a *d*-value of 35 Å between 10 °C and 20 °C and a minor broad peak at $d \approx 46$ Å. A single hydrocarbon chain correlation peak was observed in the wide-angle regime (Fig. 3B and D) in the same temperature range. Thus, hydrocarbons pack on a hexagonal lattice in the gel phase and are not tilted with respect to the membrane surface. From the position of the WAXS peak ($q_{11} = 1.51$ Å^{-1}) we calculate the area per alkyl chain (eqn (5)), $A_C = 20.1$ Å^2.

At 20 °C the sharp WAXS peak disappeared, which agrees with the chain melting transition observed by dilatometry and ultrasound velocimetry above. At the same time, the SAXS peak at $d = 46$ Å significantly increased its intensity. The diffraction pattern displayed a further peak at 23 Å (Fig. 3C), signifying lamellar order. Thus, the fluid phase is a lamellar L_α phase. The coexistence of this phase at low temperatures with the gel phase goes in hand with the broad transition width observed in dilatometry (Fig. 2C) and calorimetry.[20,25]

The structure of the gel phase described so far needs further clarification. The small *d*-value and the packing of the hydrocarbon chains suggest an interdigitated phase. To further prove this suggestion, we performed neutron scattering experiments. For neutrons, the scattering length density (SLD) of D_2O equals 6.33×10^{-6} Å^{-2}, whereas the average SLD for hydrocarbons is about -0.3×10^{-6} Å^{-2}. Thus, the significant contrast for diC14-amidine in D_2O buffer allowed us to measure the cationic liposomes in their fully hydrated state. The corresponding SANS data, shown in Fig. 4, are characteristic for positionally uncorrelated bilayers, most likely due to electrostatic repulsion imposed by the cationic lipids, leading to the formation of unilamellar vesicles.

The scattering data showed a minimum at ~0.2 Å^{-1} (Fig. 4A) relating to the zero crossing of the form factor (eqn. (7)). The observed slight shifts of its position indicate a variation in the membrane thickness with temperature. The analysis of the patterns in terms of the model described in the previous section detailed these changes. Below the main transition, the fit yielded $d_{HC} = 17.8 \pm 0.2$ Å (Fig. 4B). No phase coexistence was detected in the case of SANS. This can be explained by the small amounts of the coexisting phase (Fig. 3C) and the small differences in d_{HC}-values (Fig. 4B). The thickness obtained at 15 °C can be compared to the theoretical length of myristic chains in an all-*trans* configuration. Using 1.27 Å as the average distance between two C-bonds[40] we arrive at $d_{HC}^{calc} = 14 \times 1.27$ Å $= 17.78$ Å. The excellent agreement between d_{HC} and d_{HC}^{calc} and also the zero molecular tilt and hexagonal packing of the hydrocarbons (Fig. 3D) demonstrate that the gel phase is a lamellar interdigitated phase, $L_{\beta I}$. As the temperature was increased, d_{HC} exhibited a maximum of 20.2 Å at 20 °C and then decreased monotonously to $d_{HC} = 19.71$ Å at 30 °C.

Finally, we calculated the structural parameters for diC14-amidine, combining our results from the dilatometry, X-ray and neutron scattering data. Table 1 lists the results for two temperatures at 15 and 30 °C, *i.e.* in the $L_{\beta I}$ and L_α phases.

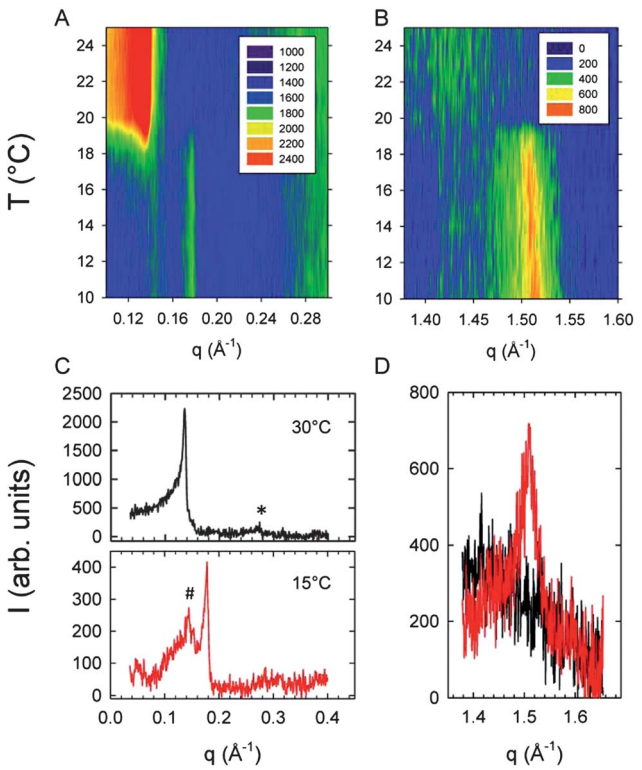

Fig. 3 SAXS (A) and WAXS (B) patterns of diC14-amidine as a function of temperature. Panel (C) shows the SAXS patterns at 15 °C and 30 °C. The corresponding WAXS patterns are shown in panel (D) (red: 15 °C, black: 30 °C). The '*' in panel (C) denotes the second lamellar order in the fluid phase and the '#' a coexisting minor phase at low temperatures.

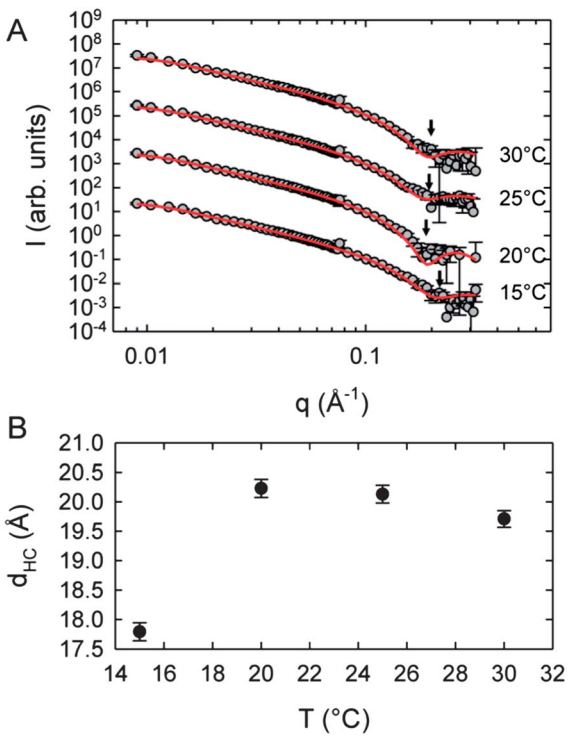

Fig. 4 Neutron scattering on diC14-amidine liposomes as a function of temperature. SANS patterns (panel (A)) were shifted vertically for better graphical presentation. Solid lines correspond to the best fit using eqn (6) and (7). Arrows indicate the minimum position of the scattered intensity. Panel (B) shows the hydrocarbon thickness of diC14-amidine resulting from this analysis.

Discussion

We have combined dilatometry, ultrasound velocity, as well as X-ray and neutron scattering to study the structural properties of diC14-amidine as a function of temperature. At low temperatures the system exhibits an interdigitated phase $L_{\beta I}$, which melts into a L_α phase at $T_m = 21.6$ °C. In order to understand the fusogenic properties of the lipid, it is instructive to compare the structural parameters to those of other lipids. Interdigitation has been reported for several lipids and can be understood in general by the delicate balance of headgroup and hydrocarbon chain interactions.[41] If repulsion in the headgroup regime overcomes the surface tension at the hydrophobic–hydrophilic interface, an interdigitated phase results. This is usually the case for lipids with large effective headgroup sizes,[42–46] or for lipid mixtures with large ions,[47] anaesthetics,[48] lysophospholipids,[49] short chain alcohols[50–54] or antimicrobial peptides.[55,56] However, if one compares the area per hydrocarbon, $A_C = 20.1$ Å^2, of diC14-amidine to that reported for other lipids forming interdigitated phases, one finds significantly lower values, *e.g.* 19.5 Å^2 was reported for diacyl-P-O-ethylphosphatidylcholines[45] and 19.3 Å^2 for dipalmitoyl phosphatidylglycerol.[36] Both lipids, like diC14-amidine, are charged (diacyl-P-O-ethylphosphatidylcholines are cationic and dipalmitoyl phosphatidylglycerol anionic), but have significantly larger headgroups. The larger A_C value of diC14-amidine is, therefore, surprising. It can be understood, however, considering the different backbones. The two lipids with the small A_C both have a glycerol backbone, *i.e.* essentially three connected carbons (*cp.* Fig. 1B). In turn, for diC14-amidine the acyl chains are attached to NH groups, which are separated by three carbons (Fig. 1A). Thus, there are two additional "spacers" between the myristic chains. Hence, the amidine headgroup composed of trimethylammonium is not the limiting factor in packing of the hydrocarbon chains. Here, the size of the backbone is responsible for the larger separation of the acyl chains and also for the formation of the $L_{\beta I}$ phase. Note that the hydrocarbon chain analogue dimyristoyl phosphatidylglycerol forms no interdigitated gel phase,[36] despite having a larger charged headgroup.

Two different packings of the hydrocarbons can be conceived. Either the amidine molecules pack side by side, flipping the molecule horizontally from one to the other lipid (Fig. 5A), or one of the two amidine chains interdigitates into the space between chains of the opposing lipid (Fig. 5B). The advantage of the latter structure would be a better shielding of the hydrophobic region from the aqueous phase. However, such a packing would require a backbone length of ~9 Å, as shown from the WAXS data (Fig. 3D). Considering typical C–C bond lengths (1.27 Å) and the structure of the amidine backbone (Fig. 1A) yields a length of only ~5 Å. Thus, the gel phase structure of diC14-amidine should be given by Fig. 5A.

At the same time this means that significant hydrophobic parts of the membrane surface are exposed to the aqueous phase. These parts are probably shielded by water that needs to adjust its network of hydrogen bonds at the interface, leading to ordered water, similar to water clathrate structures around apolar molecules.[57] Thus, electrostatic interactions between the headgroups and van der Waals interactions between the hydrocarbon chains seem to just be strong enough to stabilize a membrane. This explains qualitatively the low partial specific volume and that the melting of diC14-amidine is of low cooperativity (Fig. 2).

At the phase transition, the interdigitation of the hydrocarbon chains is abolished, as observed by the jump-like increase of the membrane thickness (Fig. 5). The then following decrease of d_{HC} with temperature is due to a progressive *trans–gauche* isomerisation of the acyl chains (melting) and has been well documented for other phospholipids.[58,59] The structure of the L_α phase of diC14-amidine can be compared to that formed by the chain analogue phospholipid DMPC (Fig. 1B), which melts at slightly higher temperatures.[26] At 30 °C, $d_{HC} = 25.4$ Å,[60] which is almost 6 Å larger than our value for diC14-amidine. Further, the lateral area per lipid of diC14-amidine (Table 1) is 7.2 Å^2 larger than that of DMPC[60] and compares better with that of dioleoyl phosphatidylcholine[61] with two unsaturated hydrocarbon chains as the main contributors to this larger area. These anomalous structural values of diC14-amidine can again be reconciled considering the long backbone of the lipid. Because of the larger spacing between the two alkyl chains, steric interactions between the hydrocarbons are small, increasing the free volume for fluctuations of the chains. Additional, partial hydrocarbon chain interdigitation can also occur. It is also interesting to compare our results to previous structural data of diC14-amidine obtained in the presence of DNA.[22] For fluid lamellar phases with

Table 1 Structural properties of diC14-amidine membranes

	$L_{\beta I}$[a]	L_α[b]
V (Å^3)	892 ± 2	898 ± 2
V_H (Å^3)	177 ± 10	177 ± 10
V_C (Å^3)	715 ± 10	721 ± 10
A (Å^2)	40.2 ± 0.2	73.2 ± 1.5
d_{HC} (Å)	17.8 ± 0.2	19.7 ± 0.2

[a] $T = 15$ °C. [b] $T = 30$ °C.

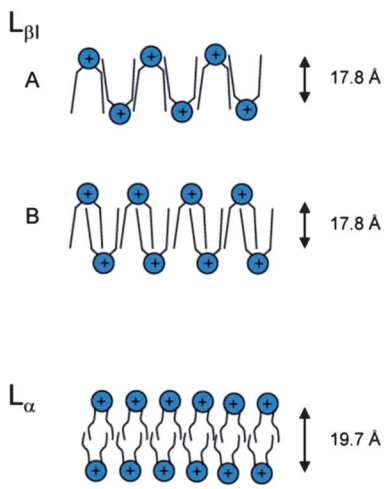

Fig. 5 Structure of the $L_{\beta I}$ and L_α phases of diC14-amidine as determined from the neutron and X-ray scattering studies. Experimental d_{HC} values are given (Table 1). Two different possible $L_{\beta I}$ structures are shown. Structural data support form (A).

intercalated DNA strands a membrane thickness of 30 Å was reported.[22] Based on the structure of the amidine headgroup (Fig. 1A), we estimate a headgroup thickness of about 5 Å. If we add twice this value to d_{HC}, we find excellent agreement with the previous report.

Finally, we consider, how these structural properties relate to the fusogenic properties of diC14-amidine. Compared to other lipids, amidine shows increased fusion to macrophage cells.[19] Most interestingly, however, recent data demonstrate increased fusion of diC14-amidine in the gel phase.[25] This temperature dependent fusogenic activity is contrary to what has been observed so far with peptides and virus-induced fusion. The cone-like molecular structure of diC14-amidine[19] explains its fusion capabilities in the fluid phase due to the larger negative curvature favouring the formation of stalk intermediate structures.[28,29] Similarly, neutral lipids, with large negative spontaneous curvatures, such as dioleoyl phosphatidylethanolamine that forms an inverted hexagonal phase in broad ranges of temperatures and osmotic pressures,[62] have been mixed with cationic lipids and found to promote gene-transfection.[2,3] The work associated with transforming lamellar lipoplexes to inverted hexagonal structures has been determined to be $\sim 1.6\ k_B T$[63] (k_B is Boltzmann's constant), which can be significantly lowered by decreasing the bending rigidity, *e.g.* by adding a short chain alcohol.

The enhanced fusion of amidine liposomes in the gel phase is puzzling, as it is coupled to the formation of an $L_{\beta I}$ phase. Standard lipid fusion requires the formation of point-like defects, *i.e.* hourglass-shaped stalk motives, which involves strong bending of one lipid leaflet in each of the two fusing bilayers.[28,29]

Certainly, this is not possible in $L_{\beta I}$ phases, where the two lipid monolayers cannot slide against each other, but are tied together (interdigitated). Consequently stalk formation would cost more energy than in the fluid phase and hence decrease the fusion probability, in contrast to experimental observation. The key to understand this property lies in the special form of the $L_{\beta I}$ structure (Fig. 5A). In "typical" $L_{\beta I}$ phases lipid headgroups are large enough to shield the hydrophobic core of the membrane (see, *e.g.*, ref. 36). Here, we found that a significant amount of hydrophobic entities of the $L_{\beta I}$ phase of diC14-amidine will be exposed to the aqueous phase. This makes this phase rather unstable as compared to conventional interdigitated phases. For fusion, such a structure is, however, energetically favourable, because interfacial water bound to amidine can easily be removed. In fact, we would expect even a positive entropic contribution to fusion from the release of the water bound at the non-polar regions. Based on these considerations we propose a novel fusion mechanism schematically drawn in Fig. 6.

The fusion process starts as usual by an attraction between the target and the amidine membrane, due to electrostatic interactions between the cationic lipids and anionic moieties of the target membrane, *e.g.* glycolipids (stage I). Attraction is further supported by (i) negligible bending fluctuations, and hence insignificant steric repulsion,[64] of the amidine membranes in the gel phase as compared to the fluid phase and (ii) gain in entropy by releasing water that shields the apolar parts of the $L_{\beta I}$ phase.

At stage II, amidine lipids, which face the target membrane with their hydrophobic tails, will enter the opposing membrane and lead to an asymmetric expansion and membrane bending,

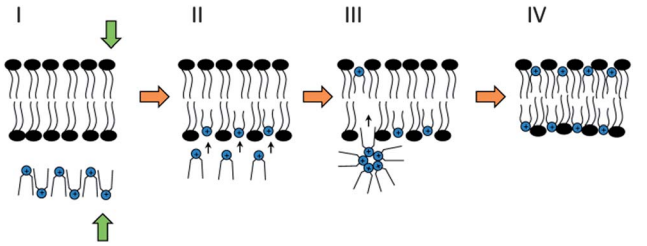

Fig. 6 Fusion of amidine membranes in the $L_{\beta I}$ phase with a lipid bilayer. At stage (I) the two membranes attract each other, *e.g. via* electrostatic interactions. The intermediate stage (II) is unstable and shows the incorporation of amidine molecules with their hydrophobic entities facing the opposing membrane leading to a lateral expansion and/or bending of the target membrane. The remaining amidine lipids may transiently form unstable inverted micellar aggregates or directly dissolve into the target membrane (III). Final equilibration is achieved by lateral diffusion and flip-flop processes (IV).

which can be compensated by flip-flop mechanisms. The remaining amidine molecules in the aqueous phase may spontaneously aggregate, *e.g.* into inverted micelles (stage III), and then dissolve into the target membrane or enter the membrane directly by flipping horizontally. Finally the system equilibrates by lateral expansion and lipid flip-flops (stage IV).

Conclusions

Based on our structural results on diC14-amidine, we propose a novel fusion mechanism to explain the increased fusion capability of the lipid in the gel phase. We encourage theoretical and simulation studies on this fusion process to detail the involved energetic contributions and molecular rearrangements. This will also help to show whether this mechanism is generic or specific to amidine. Good candidates for experimental tests are diacyl-P-O-ethylphosphatidylcholines, which are cationic lipids that form $L_{\beta I}$ phases.[45]

Acknowledgements

The authors are thankful to V. A. Raghunathan for helpful discussions and to Michael Rappolt and Karl Lohner for critical reading of the manuscript. This work is based partly on experiments performed at the Jülich Centre for Neutron Science JCNS, Forschungszentrum Jülich, Germany and the Laboratoire Léon-Brillouin CEA/CNRS Saclay, France. The authors acknowledge both facilities for the provision of neutron beam time at their instruments. We further thank Dumitru Macovei for technical assistance in SAXS experiments. CL and MV are postdoctoral researcher and research associate, respectively, at the FNRS (Belgium).

Notes and references

1 J. O. Radler, I. Koltover, T. Salditt and C. R. Safinya, *Science*, 1997, **275**, 810–814.
2 I. Koltover, T. Salditt, J. O. Radler and C. R. Safinya, *Science*, 1998, **281**, 78–81.
3 R. Podgornik, D. Harries, V. A. Parsegian and H. H. Strey, in *Gene-Therapy-Therapeutic Mechanisms and Strategies*, ed. N. Smyth-Templeton, Marcel Dekker, New York (NY), 2003, pp. 301–332.

4 R. Krishnaswamy, V. A. Raghunathan and A. K. Sood, *Phys. Rev. E: Stat., Nonlinear, Soft Matter Phys.*, 2004, **69**, 031905.
5 R. Krishnaswamy, G. Pabst, M. Rappolt, V. A. Raghunathan and A. K. Sood, *Phys. Rev. E: Stat., Nonlinear, Soft Matter Phys.*, 2006, **73**, 031904.
6 K. K. Ewert, H. M. Evans, A. Zidovska, N. F. Bouxsein, A. Ahmad and C. R. Safinya, *J. Am. Chem. Soc.*, 2006, **128**, 3998–4006.
7 P. L. Felgner, T. R. Gadek, M. Holm, R. Roman, H. W. Chan, M. Wenz, J. P. Northrop, G. M. Ringold and M. Danielsen, *Proc. Natl. Acad. Sci. U. S. A.*, 1987, **84**, 7413–7417.
8 A. Elouahabi and J. M. Ruysschaert, *Mol. Ther.*, 2005, **11**, 336–347.
9 L. Wasungu and D. Hoekstra, *J. Controlled Release*, 2006, **116**, 255–264.
10 C. R. Safinya, K. Ewert, A. Ahmad, H. M. Evans, U. Raviv, D. J. Needleman, A. J. Lin, N. L. Slack, C. George and C. E. Samuel, *Philos. Trans. R. Soc., A*, 2006, **364**, 2573–2596.
11 C. Tros de Ilarduya, Y. Sun and N. Duzgunes, *Eur. J. Pharm. Sci.*, 2010, **40**, 159–170.
12 J. M. Ruysschaert, A. El Ouahabi, V. Willeaume, G. Huez, R. Fuks, M. Vandenbranden and P. Di Stefano, *Biochem. Biophys. Res. Commun.*, 1994, **203**, 1622–1628.
13 A. El Ouahabi, V. Pector, R. Fuks, M. Vandenbranden and J. M. Ruysschaert, *FEBS Lett.*, 1996, **380**, 108–112.
14 J. M. Ruysschaert, *Cell. Mol. Biol. Lett.*, 2002, **7**, 249–250.
15 C. Lonez, M. Vandenbranden and J. M. Ruysschaert, *Prog. Lipid Res.*, 2008, **47**, 340–347.
16 T. Tanaka, A. Legat, E. Adam, J. Steuve, J. S. Gatot, M. Vandenbranden, L. Ulianov, C. Lonez, J. M. Ruysschaert, E. Muraille, M. Tuynder, M. Goldman and A. Jacquet, *Eur. J. Immunol.*, 2008, **38**, 1351–1357.
17 C. Lonez, A. Legat, M. Vandenbranden and J. M. Ruysschaert, *Cell. Mol. Life Sci.*, 2008, **65**, 620–630.
18 C. Lonez, M. Vandenbranden, M. Ouali, A. Legat, J. M. Ruysschaert and A. Elouahabi, *Mol. Membr. Biol.*, 2006, **23**, 227–234.
19 C. Lonez, M. F. Lensink, E. Kleiren, J. M. Vanderwinden, J. M. Ruysschaert and M. Vandenbranden, *Cell. Mol. Life Sci.*, 2010, **67**, 483–494.
20 V. Pector, J. Caspers, S. Banerjee, L. Deriemaeker, R. Fuks, A. El Ouahabi, M. Vandenbranden, R. Finsy and J. M. Ruysschaert, *Biochim. Biophys. Acta*, 1998, **1372**, 339–346.
21 V. Pector, J. Backmann, D. Maes, M. Vandenbranden and J. M. Ruysschaert, *J. Biol. Chem.*, 2000, **275**, 29533–29538.
22 V. Cherezov, H. Qiu, V. Pector, M. Vandenbranden, J. M. Ruysschaert and M. Caffrey, *Biophys. J.*, 2002, **82**, 3105–3117.
23 M. F. Lensink, C. Lonez, J. M. Ruysschaert and M. Vandenbranden, *Langmuir*, 2009, **25**, 5230–5238.
24 C. R. Benatti, R. P. Barroso, C. Lonez, J. M. Ruysschaert and M. T. Lamy, *Biochim. Biophys. Acta*, 2009, **1788**, 1304–1309.
25 T. R. Oliveira, E. L. Duarte, M. T. Lamy, M. Vandenbranden, J. Ruysschaert and C. Lonez, *Langmuir*, 2012, **28**, 4640–4647.
26 R. Koynova and M. Caffrey, *Biochim. Biophys. Acta*, 1998, **1376**, 91–145.
27 C. R. Benatti, J. M. Ruysschaert and M. T. Lamy, *Chem. Phys. Lipids*, 2004, **131**, 197–204.
28 D. P. Siegel, *Biophys. J.*, 1999, **76**, 291–313.
29 L. K. Tamm, J. Crane and V. Kiessling, *Curr. Opin. Struct. Biol.*, 2003, **13**, 453–466.
30 L. V. Chernomordik and M. M. Kozlov, *Nat. Struct. Mol. Biol.*, 2008, **15**, 675–683.
31 P. Laggner and H. Stabinger, in *Colloid and Interface Science*, ed. M. Kerker, Academic Press, New York, 1976, pp. 91–96.
32 A. P. Sarvazyan, *Ultrasonics*, 1982, **20**, 151–154.
33 T. J. McIntosh and S. A. Simon, *Biochemistry*, 1986, **25**, 4948–4952.
34 J. F. Nagle and S. Tristram-Nagle, *Biochim. Biophys. Acta*, 2000, **1469**, 159–195.
35 H. I. Petrache, S. Tristram-Nagle, K. Gawrisch, D. Harries, V. A. Parsegian and J. F. Nagle, *Biophys. J.*, 2004, **86**, 1574–1586.
36 G. Pabst, S. Danner, S. Karmakar, G. Deutsch and V. A. Raghunathan, *Biophys. J.*, 2007, **93**, 513–525.
37 D. P. Kharakoz, A. Colotto, K. Lohner and P. Laggner, *J. Phys. Chem.*, 1993, **97**, 9844–9851.
38 T. Heimburg, *Biochim. Biophys. Acta*, 1998, **1415**, 147–162.
39 S. Mabrey and J. M. Sturtevant, *Proc. Natl. Acad. Sci. U. S. A.*, 1976, **73**, 3862–3866.
40 W. J. Sun, S. Tristram-Nagle, R. M. Suter and J. F. Nagle, *Biophys. J.*, 1996, **71**, 885–891.
41 J. F. Nagle, *Annu. Rev. Phys. Chem.*, 1980, **31**, 157–195.
42 J. L. Ranck, T. Keira and V. Luzzati, *Biochim. Biophys. Acta*, 1977, **488**, 432–441.
43 P. Laggner, K. Lohner, G. Degovics, K. Muller and A. Schuster, *Chem. Phys. Lipids*, 1987, **44**, 31–60.
44 P. Laggner, K. Lohner, R. Koynova and B. Tenchov, *Chem. Phys. Lipids*, 1991, **60**, 153–161.
45 I. Winter, G. Pabst, M. Rappolt and K. Lohner, *Chem. Phys. Lipids*, 2001, **112**, 137–150.
46 S. Tristram-Nagle, R. N. Lewis, J. W. Blickenstaff, M. Diprima, B. F. Marques, R. N. McElhaney, J. F. Nagle and J. W. Schneider, *Chem. Phys. Lipids*, 2005, **134**, 29–39.
47 B. A. Cunningham, P. J. Quinn, D. H. Wolfe, W. Tamura-Lis, L. J. Lis, O. Kucuk and M. P. Westerman, *Biochim. Biophys. Acta*, 1995, **1233**, 68–74.
48 T. Hata, H. Matsuki and S. Kaneshina, *Biophys. Chem.*, 2000, **87**, 25–36.
49 J. Z. Lu, Y. H. Hao and J. W. Chen, *J. Biochem.*, 2001, **129**, 891–898.
50 T. J. McIntosh, R. V. McDaniel and S. A. Simon, *Biochim. Biophys. Acta*, 1983, **731**, 109–114.
51 E. S. Rowe, *Biochim. Biophys. Acta*, 1985, **813**, 321–330.
52 T. Adachi, H. Takahashi, K. Ohki and I. Hatta, *Biophys. J.*, 1995, **68**, 1850–1855.
53 T. J. McIntosh, H. Lin, S. Li and C. Huang, *Biochim. Biophys. Acta*, 2001, **1510**, 219–230.
54 M. Kranenburg, M. Vlaar and B. Smit, *Biophys. J.*, 2004, **87**, 1596–1605.
55 E. Sevcsik, G. Pabst, A. Jilek and K. Lohner, *Biochim. Biophys. Acta*, 2007, **1768**, 2568–2595.
56 E. Sevcsik, G. Pabst, W. Richter, S. Danner, H. Amenitsch and K. Lohner, *Biophys. J.*, 2008, **94**, 4688–4699.
57 J. Israelachvili, *Intermolecular and Surface Forces*, Academic Press, London, 1991.
58 G. Pabst, J. Katsaras, V. A. Raghunathan and M. Rappolt, *Langmuir*, 2003, **19**, 1716–1722.
59 G. Pabst, H. Amenitsch, D. P. Kharakoz, P. Laggner and M. Rappolt, *Phys. Rev. E: Stat., Nonlinear, Soft Matter Phys.*, 2004, **70**, 021908.
60 N. Kucerka, Y. Liu, N. Chu, H. I. Petrache, S. Tristram-Nagle and J. F. Nagle, *Biophys. J.*, 2005, **88**, 2626–2637.
61 J. Pan, S. Tristram-Nagle, N. Kucerka and J. F. Nagle, *Biophys. J.*, 2008, **94**, 117–124.
62 R. P. Rand, N. L. Fuller, S. M. Gruner and V. A. Parsegian, *Biochemistry*, 1990, **29**, 76–87.
63 D. Danino, E. Kesselman, G. Saper, H. I. Petrache and D. Harries, *Biophys. J.*, 2009, **96**, L43–L45.
64 W. Helfrich, *Z. Naturforsch., A: Phys. Phys. Chem. Kosmophys.*, 1978, **33a**, 305–315.

Addition and correction

Note from RSC Publishing

This article was originally published with incorrect page numbers. This is the corrected, final version.

The Royal Society of Chemistry apologises for these errors and any consequent inconvenience to authors and readers.